Environmental Science & Technology

Article

Cite This: Environ. Sci. Technol. XXXX, XXX, XXX−XXX

pubs.acs.org/est

Tomographic Reservoir Imaging with DNA-Labeled Silica Nanotracers: The First Field Validation

Xiang-Zhao Kong,*[,†] Claudia A. Deuber,[†] Anniina Kittilä,[†] Márk Somogyvári,[‡] Gediminas Mikutis,[¶] Peter Bayer,[§] Wendelin J. Stark,[¶] and Martin O. Saar[†]

[†]Geothermal Energy and Geofluids Group, Department of Earth Sciences, ETH Zurich, 8092 Zurich, Switzerland

[‡]Institute of Mathematics, University of Potsdam, 14476 Potsdam-Golm, Germany

[¶]Functional Materials Laboratory, Department of Chemistry and Applied Biosciences, ETH Zurich, 8093 Zurich, Switzerland

[§]Institute of new Energy Systems (InES), Ingolstadt University of Applied Sciences, 85049 Ingolstadt, Germany

Supporting Information

ABSTRACT: This study presents the first field validation of using DNA-labeled silica nanoparticles as tracers to image subsurface reservoirs by travel time based tomography. During a field campaign in Switzerland, we performed short-pulse tracer tests under a forced hydraulic head gradient to conduct a multisource−multireceiver tracer test and tomographic inversion, determining the two-dimensional hydraulic conductivity field between two vertical wells. Together with three traditional solute dye tracers, we injected spherical silica nanotracers, encoded with synthetic DNA molecules, which are protected by a silica layer against damage due to chemicals, microorganisms, and enzymes. Temporal moment analyses of the recorded tracer concentration breakthrough curves (BTCs) indicate higher mass recovery, less mean residence time, and smaller dispersion of the DNA-labeled nanotracers, compared to solute dye tracers. Importantly, travel time based tomography, using nanotracer BTCs, yields a satisfactory hydraulic conductivity tomogram, validated by the dye tracer results and previous field investigations. These advantages of DNA-labeled nanotracers, in comparison to traditional solute dye tracers, make them well-suited for tomographic reservoir characterizations in fields such as hydrogeology, petroleum engineering, and geothermal energy, particularly with respect to resolving preferential flow paths or the heterogeneity of contact surfaces or by enabling source zone characterizations of dense nonaqueous phase liquids.

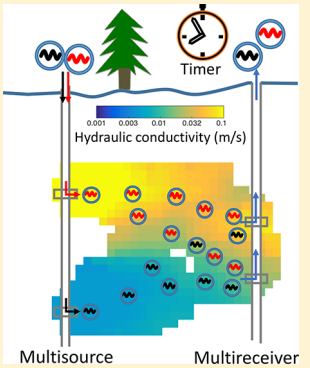

INTRODUCTION

Hydrogeologic conditions are often investigated by employing pumping tests[1−4] as well as both artificial[5−7] and natural[7−12] tracer tests. Such tests are also frequently employed to characterize petroleum or geothermal reservoirs. Data from such tests are utilized in analytical[12−14] and numerical[15,16] models to further improve the prediction of subsurface mass and energy transport.

While the conventional analysis of the breakthrough curve (BTC) of a single-tracer test can yield bulk flow and transport properties of reservoirs,[7,17−19] it is difficult to use this method to capture the spatial heterogeneities of hydraulic properties without additional measurements. However, following a similar tomographic procedure as employed in geophysics,[20−22] where the subsurface structure is imaged, employing a computational reconstruction on projection series recorded from different angles, or during hydraulic tomography,[23−29] where subsurface hydraulic parameters are reconstructed via the inversion of fluid pressure data from a series of hydraulic tests, spatial heterogeneities of hydraulic properties (e.g., hydraulic conductivity fields, K) may be resolved when employing multiple tracers during tracer-based tomography.[30] However, such tomography requires the concurrent use of multiple distinguishable, but in a transport environment, close to identically behaving tracers. In tracer tomography, one uniquely identifiable tracer type is used per injection location and all tracer types are collected at multiple observation locations. Thereafter, BTCs may be obtained to delineate preferential fluid flow pathways.[18,31,32] Moreover, compared to hydraulic tomography, tracer tomography is capable of revealing additional reservoir features, such as the heterogeneity of contact surfaces[33,34] and enables source zone characterizations of dense nonaqueous phase liquids.[17,18,35]

Despite the tremendous application potential of traditional tracers, such as natural silica, stable isotopes, bromide, and fluorescent dyes, these tracers have been reported to suffer from interference of background noise,[36−38] low detection sensitivity due to dilution effects,[39,40] high analysis costs,[41,42] potential environmental contamination,[43,44] signal "contamination", and limited availability of multiple similar tracer variants during tracer tomography.[6,31,45] Alternatively, nanotechnology[38,46,47] has developed tracers that can carry synthetic deoxyribonucleic acid (DNA) molecules, which

Received: August 6, 2018
Revised: October 26, 2018
Accepted: November 2, 2018
Published: November 2, 2018

Downloaded via ETH ZURICH on November 19, 2018 at 11:26:31 (UTC).
See https://pubs.acs.org/sharingguidelines for options on how to legitimately share published articles.

ACS Publications © XXXX American Chemical Society

DOI: 10.1021/acs.est.8b04367
Environ. Sci. Technol. XXXX, XXX, XXX−XXX

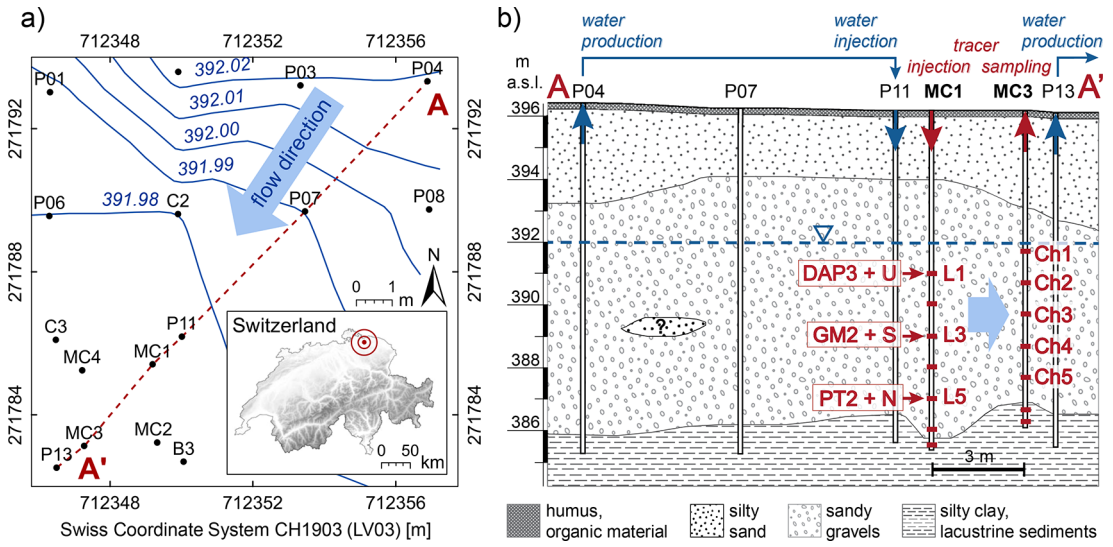

Figure 1. (a) Map of the Widen hydrogeology field test site in northern Switzerland and (b) Cross section of the test line A−A' depicted in panel a. The hydraulic head distribution during the forced hydraulic head gradient tracer test is shown by blue isolines (in m a.s.l.). The inset figure shows a shaded relief map of Switzerland, where darker colors represent higher elevations (source: Swiss Federal Office of Topography). The Widen site is marked as a red point. The cross-sectional profile in panel b includes the water table (blue-dashed line) as well as the DNA nanotracer (DAP3, GM2, PT2) and solute dye tracer (U, S, N) injection and sampling locations, where U is uranine, S is sulforhodamine B, and N is Na-naphthionate. Tracers are injected at (from top to bottom) levels L1 (391.05 m a.s.l.), L3 (389.05 m a.s.l.), and L5 (387.05 m a.s.l.) of injection well MC1. Tracers are sampled at channels Ch1 (391.70 m a.s.l.), Ch2 (390.70 m a.s.l.), Ch3 (389.70 m a.s.l.), Ch4 (388.70 m a.s.l.), and Ch5 (387.70 m a.s.l.) of sampling well MC3.

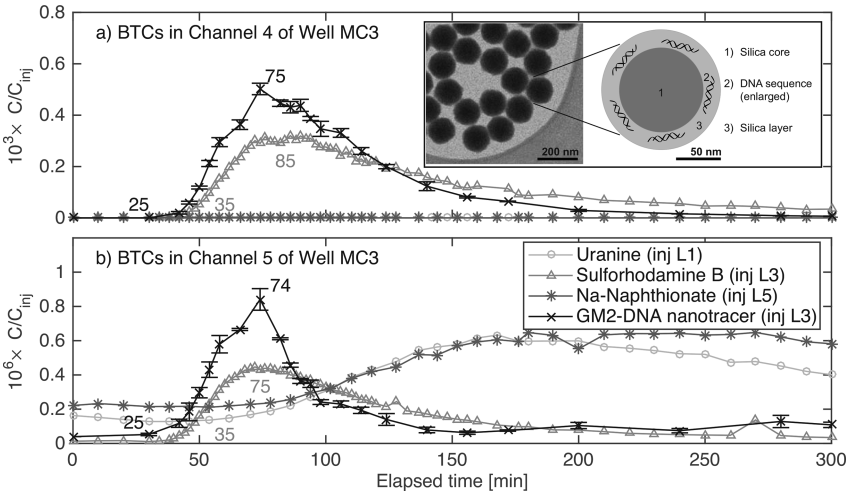

Figure 2. Results of the field experiment at the Widen hydrogeology field test site (Figure 1). (a and b) BTCs in sampling channels Ch4 and Ch5, respectively, recorded in the sampling well (MC3). The first and peak arrival times of sulforhodamine B and GM2-DNA nanotracer are given in minutes. Error bars of DNA nanotracer BTCs show the standard deviation of concentration measurements. For plotting cleanness, standard deviations (in general less than 1% of the measured concentration) of solute tracers are not shown. Channels Ch1−Ch3 of sampling well MC3 do not record any signal (see Supporting Information for more details). (a inset) Scanning transmission electron microscope (STEM) image and schematic of a DNA nanotracer (with a diameter of about 150 nm) used in this study.

have the potential to provide an effective solution to address these challenges. DNA tracers have been reported to be specific (i.e., bearing unique identifiers that do not suffer from interference by background noise), environmentally friendly, ultrasensitive to detection, and multiplex capable (i.e., enabling concurrent usage of a large number of species at a given time).[38,48−52] These characteristics enable the concurrent use of multiple DNA tracers, each with a unique DNA sequence, to identify sources and pathways of different water bodies. Importantly, DNA tracers can be repetitively and thus exponentially amplified, using quantitative polymerase chain reaction (qPCR), theoretically pushing the detection sensitivity down to one molecule.[38,52,53] Hence, tracers containing DNA require a detection amount that is orders of magnitude lower than that of traditional tracers.[49,52] Furthermore, the fabrication and qPCR analysis of DNA tracers have been reported to be rapid and cost-effective.[38,47,49,52] These features of DNA tracers has led to their extensive use during fluid tracing investigations, such as column experiments,[50,52,54] streamwater tracing,[55−57] groundwater tracing in karst systems,[50,58] and tracer tests in porous and fractured aquifers.[52−54,59,60]

In this study, we report on the first tomographic imaging of an unconsolidated aquifer using DNA-labeled silica nano-

DOI: 10.1021/acs.est.8b04367
Environ. Sci. Technol. XXXX, XXX, XXX−XXX

Table 1. Properties of the DNA Nanotracers and Results of the Temporal Moment Analysis[a]

DNA nanotracersDNA nanotracers	base pairs	size [nm]	ζ-potential [mV]	mass recovery ratio[b]	mean residence time ratio[c]	dispersion ratio[d]
DAP3	108	141 ± 24	−42.5 ± 0.4	n/a	n/a	n/a
PT2	120	145 ± 27	−39.9 ± 1.0	n/a	n/a	n/a
GM2	76	159 ± 23	−45.1 ± 0.2	1.04 in Ch4	0.79 in Ch4	0.61 in Ch4
				1.23 in Ch5	0.97 in Ch5	1.04 in Ch5

[a]The particle density is about 2.1 g/cm^3. All DNA sequences are double-stranded. DNA forward and reverse primers are listed in the Supporting Information (Table S1 and Figure S1). The comparison between DNA nanotracers and sulforhodamine B is accomplished by analyzing the temporal moments of the respective BTCs,[52,66] using normalized concentrations $\overline{c} = C/C_{inj}$, where C and C_{inj} are the measured tracer concentration in sampling well MC3 and the injected tracer concentration in injection well MC1, respectively. n/a: not applicable. Subscripts "DNA" and "S" refer to DNA nanotracers and sulforhodamine B dye tracer. [b]Defined as $\left(\int \overline{c}\,dt\right)_{DNA} \Big/ \left(\int \overline{c}\,dt\right)_{S}$. [c]Defined as $\left(\frac{\int t\overline{c}\,dt}{\int \overline{c}\,dt}\right)_{DNA} \Big/ \left(\frac{\int t\overline{c}\,dt}{\int \overline{c}\,dt}\right)_{S}$. [d]Defined as $\left(\frac{\int t^2\overline{c}\,dt}{\int \overline{c}\,dt}\right)_{DNA} \Big/ \left(\frac{\int t^2\overline{c}\,dt}{\int \overline{c}\,dt}\right)_{S}$

particles (henceforth referred to as DNA nanotracers). The key objective of this study is to validate and advance the application of DNA nanotracers in field tracer tomography. In the following, we first present the study site, the DNA nanotracers, and the methods used during our 2016 field campaign. We then document the measured BTCs and compare the results of a temporal moment analysis and travel-time tomography between DNA nanotracers and solute dye tracers. To conclude our study, we also compare our hydrogeology findings with the ones from previous investigations at the same site.

STUDY SITE, MATERIALS, AND METHODS

The Widen Site. Our field tests in 2016 took place at the Widen site in a flat valley next to the Thur River in northern Switzerland (Figure 1). Previous studies[20,21,31,32] have documented the following horizontal geological layers (with increasing depth) at that site:

(i) 10 cm thick layer of humus and organic material (396 m a.s.l.);
(ii) 2−3 m thick layer of well sorted silty sand with some clay (flood sediments);
(iii) 7 m thick layer of sandy gravel with some fine materials, well-graded and well-rounded components, Thur-valley gravel (German: Thurtalschotter); in addition, some sand lenses with low permeability are present, which have the same composition as the sand layer above;
(iv) Below the sandy gravel (from a borehole depth of 10 m downward), silty clay as well as lacustrine sediments.

The groundwater table is generally within the Thurtalschotter layer and is directly affected by the water table of the Thur River. The predominant groundwater flow direction is indicated by a blue arrow in Figure 1. However, previous studies[32] have reported deviations of the groundwater flow direction of up to 45°. Therefore, to stabilize the groundwater flow direction and to align it with injection well MC1 and with sampling well MC3, the natural hydraulic head gradient is modified by pumping water from well P04 into well P11 (at ∼0.2 L/s) and from well P13 (at ∼ − 0.8 L/s), discharging it sufficiently far away from the investigation site to avoid aquifer recharge. Figure 1 illustrates the resultant water table and hydraulic head gradient during the field test.

Tracers and Their Analyses. During the field test, three different mixtures of tracers, each with a volume of 1 L, are simultaneously injected as a short-pulse input (with a duration of 20−30 s) as follows: 1 g of uranine plus 0.2 g of DAP3-DNA nanotracer at L1, 4 g of sulforhodamine B plus 0.2 g of GM2-DNA nanotracer at L3, and 20 g of Na-naphthionate plus 0.2 g of PT2-DNA nanotracer at L5 (Figure 1). The injection concentrations are then 1.0, 0.2, 4, 0.2, 20.0, and 0.2 g/L of uranine, DAP3-DNA nanotracer, sulforhodamine B, GM2-DNA nanotracer, Na-naphthionate, and PT2-DNA nanotracer, respectively. The DNA nanotracers used in this study are provided by the Functional Materials Laboratory in the Institute of Chemical and Bioengineering at ETH Zurich, Switzerland.[47,61−63] The inset in Figure 2a shows a scanning transmission electron microscope (STEM) image of representative samples of the DNA nanotracers used in this study. DNA nanotracers are synthesized in three steps:[46,63] (1) silica particles, with sizes of 133 ± 4 nm, are "functionalized," resulting in a positive charge; (2) negatively charged, double-stranded DNA molecules are attached to the particles; (3) silica layers (5−10 nm thick) are grown to encapsulate and protect the DNA against environmental interaction due to chemicals, microorganisms, and enzymes. The resultant silica particles are close to spherical and have a negative surface charge,[46,63] similar to most rocks in neutral to alkaline formation fluids (following the concept of point of zero charge).[64] We use double-stranded DNA to enhance its robustness.[52,65] The silica encapsulation procedure greatly improves the stability of DNA nanotracers, compared to naked DNAs, used in several previous studies.[50,53,54,56] Properties of the DNA nanotracers are listed in Table 1 and in Table S1 of the Supporting Information.

At specific time intervals during the field tests, we take water samples with bottles (60 mL) from well MC3 at five channels, Ch1−Ch5, at elevations of 391.70 down to 387.70 m a.s.l., spaced at an even interval of 1 m in between (Figure 1). The samples are analyzed twice in the laboratory, first to measure the concentration of the three solute dye tracers, using a Luminescence Spectrometer (PerkinElmer, LS 50 B), and second to determine the identity and amount of DNA nanotracers, employing qPCR (SYBR Green-based Roche LightCycler96). Prior to the qPCR measurements, a buffered fluoride solution (0.23 g NH_4FHF (pure, Merck) plus 0.19 g NH_4F (puriss, Sigma-Aldrich) in 10 mL Milli-Q water yielding ∼25 000 ppm F-ions) is diluted to a 1% concentration (i.e., ∼250 ppm F-ions) and added to each water sample. This procedure dissolves the silica nanoparticles (within seconds) and recovers the DNA. During the qPCR measurement, the water sample is mixed with qPCR reagents (qPCR Mastermix and the DNA primers, see Table S1 in the Supporting Information) to measure its qPCR threshold cycle (Cq) number. By comparing the Cq number to a fit of a known

DOI: 10.1021/acs.est.8b04367
Environ. Sci. Technol. XXXX, XXX, XXX−XXX

concentration dilution curve (ranging between 1 ppt to 100 ppm, see Figure S2 in the Supporting Information), the Cq number is then converted to the absolute nanotracer (particle) concentration.[63] All qPCR measurements are performed in triplicates with a detection limit of roughly 10 ppt.

Moment and Travel Time Analyses. We first perform temporal moment analyses (equations listed in Table 1) on the recorded BTCs. These analyses describe the attenuation and transport characteristics of tracers during their migration through the pore space. We then interpret the recorded BTCs, using a travel time based tomographic inversion approach, following the procedures presented in detail by Somogyvari et al.,[67] who used thermal tracers (i.e., heat). Given an estimated breakthrough time, t_b, of ∼80 min (Figure 2), a distance, L, of 3 m between the two wells, and a molecular diffusion coefficient, D_m, of 10^{-9} m^2/s (for DNA nanotracers, D_m is even smaller), the Peclet number, $Pe = L^2/(t_b D_m)$, is on the order of 10^6. The transport of tracers is thus assumed to be dominated by advection. Given this assumption, tracer travel times, t_T, can be used to derive hydraulic conductivity, K, profiles of the aquifer. By transforming the transport equation into a form of the eikonal equation,[68] the tracer travel time, i.e., the tracer peak arrival time during the spreading of a tracer pulse, can be related to the inverse of the mean velocity by employing a line integral along the tracer trajectories, s, between the injection point, x_s, and the observation point, x_r, given as

$$t_T(x_r) = \int_{x_s}^{x_r} \frac{\phi(s)}{K(s)\nabla h(s)}\,\mathrm{d}s \tag{1}$$

Here, ϕ is porosity, ∇h is the hydraulic head gradient (here $\nabla h = 2.5 \times 10^{-3}$, maintained by pumping), and x_s and x_r are the source and receiver coordinates, respectively. This travel time equation contains information along one vertical cross section between the injection and the observation wells. The line integral eq 1 expresses the relationship between the travel times and the hydraulic conductivities along one transport trajectory. A set of eq 1, from multiple trajectories between multiple sources and receivers, forms an inverse problem that can be used to calculate the distribution of hydraulic conductivities. As we employ three tracer injection depths (sources) and five tracer sampling depths (receivers), crossing connection lines between sources and receivers within the vertical cross section, enable a low-resolution tomographic inversion of the 2D hydraulic conductivity field between the injection and the sampling wells. For inversion, the SIRT (simultaneous iterative reconstruction technique) algorithm is employed, which has been implemented in the software GeoTOM3D.[69] The staggered grid method is applied for model discretization, which is also adopted in related tomography applications.[28,45,67] Note that the values of hydraulic conductivity of an aquifer typically span orders of magnitude, while the variation of porosity is generally much smaller. Therefore, in the calculation of the tracer travel time in eq 1, porosity can be approximated by a constant value. This approximation has been reported to only introduce minor variations into the calculation of hydraulic conductivities.[67] The SIRT algorithm iteratively computes the transport trajectories over a discretized grid of mean velocities until the computed and observed travel times closely match. Later the computed mean velocity distribution is converted to the hydraulic conductivity field.[28,32,45,67]

RESULTS AND DISCUSSION

Breakthrough Curves. In total, three tracer tests are conducted at the Widen field site. There are 6 months between the first two tests and ∼1.5 months between the second and the third test. The first two tests fail. One reason for these failures is that, without the aforementioned groundwater injection approach, to avoid unexpected and significant deviations of the hydraulic head gradient from the long-term average, the naturally deviated hydraulic head gradient results in no tracer recovery at the sampling well. Another reason is the chemical composition of the groundwater and high bacterial activity, resulting in partial dissolution and biofilm enclosure of the DNA nanotracers.[63] To mitigate the DNA degradation, thereby enhancing the quality of the tracer signal, water samples are cooled and analyzed as soon as possible after collection. The experience gained from these two failed experiments enabled conducting the third field experiment successfully, which is presented here.

As shown in Figure 2, the third field test provides two sets of plausible BTCs that could be compared to each other: the signals of sulforhodamine B and GM2-DNA nanotracer (injected at L3 in MC1), which are recorded in observation channels Ch4 and Ch5 in MC3. In contrast, channels Ch1 to Ch3 do not yield any tracer signal (see Figure S3 in the Supporting Information). BTCs in Ch4 indicate a good hydraulic connectivity between L3 in MC1 and Ch4 in MC3, with a vertical offset of 0.35 m and a horizontal distance of 3 m (Figure 1). Tracers originating from L3 in MC1 and yielding BTCs in Ch5 in MC3, show first and peak arrival times that are almost identical to those of the BTCs obtained from Ch4 in MC3, albeit at much lower concentrations. Therefore, compared to the hydraulic connectivity between L3 in MC1 and Ch4 in MC3, a similar hydraulic connectivity is expected between L3 in MC1 and Ch5 in MC3, with a vertical offset of 1.35 m and a horizontal distance of 3 m. In Ch5, tracers of uranine and Na-naphthionate yield low-concentrations and incomplete BTCs with late arrivals. Several previous studies,[31,32] conducted at the Widen field site, have suggested a thin, low-conductivity, sand-rich layer at the depth of L2. Such a low-conductivity layer could impede the hydraulic communication between the top levels (L1 and L2) in the injection well (MC1) and the lower levels (Ch3, Ch4, and Ch5) in the sampling well (MC3). Given that uranine is injected at L1 in MC1 (Figure 1) and does not yield any meaningful signal in Ch1−Ch4, we conclude that the observed signal of uranine in Ch5 could result from (1) tracer residue, due to previous tracer studies that have been conducted at this heavily used hydrogeology field test site, as uranine is known to exhibit some sorption in porous media,[70,71] and (2) three-dimensional heterogeneity due to the low-conductivity layer at L2. At a depth significantly below L1, Na-naphthionate and PT2-DNA nanotracer are injected simultaneously at L5 in MC1 (Figure 1); however, only the Na-naphthionate solute dye tracer is detected in the bottom channel (Ch5) of the sampling well (MC3). Given that Na-naphthionate is considered to be a conservative tracer,[71] it could indeed be a late arrival of the Na-naphthionate, i.e., not a residue. The late arrival of the solute dye tracer Na-naphthionate and no arrival of the PT2-DNA nanotracer at Ch5 suggest a low hydraulic connectivity between L5 in MC1 and Ch5 in MC3.

Figure 2 shows that the GM2-DNA nanotracer in Ch4 exhibits earlier first and peak arrivals than sulforhodamine B.

DOI: 10.1021/acs.est.8b04367
Environ. Sci. Technol. XXXX, XXX, XXX−XXX

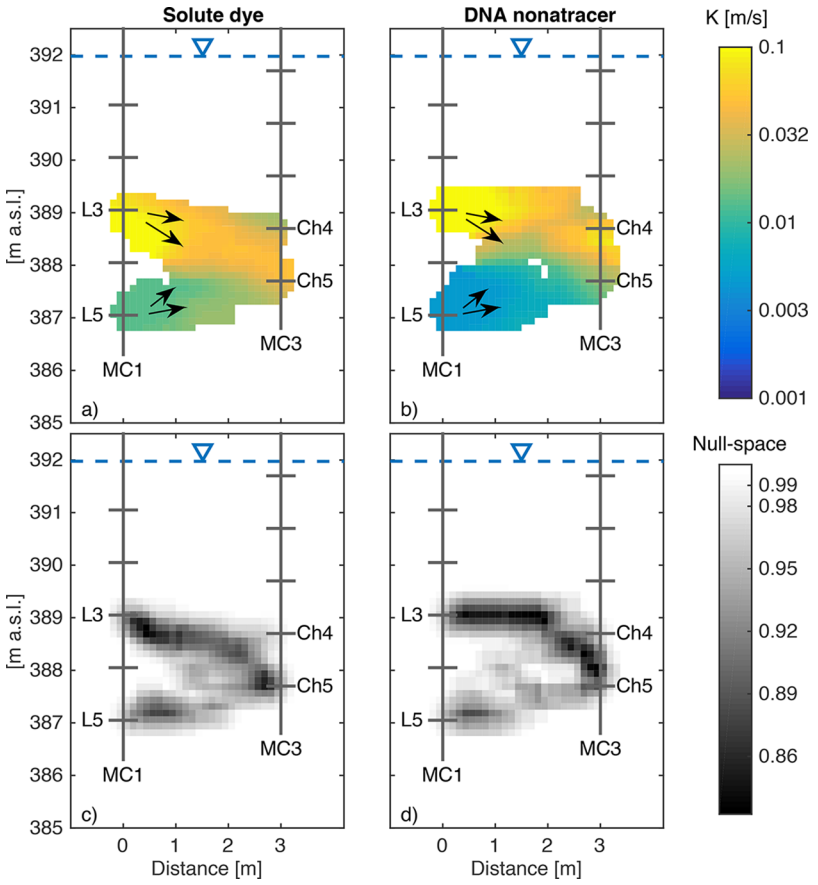

Figure 3. Results of the tomographic inversion for solute dye tracers (left column) and particulate DNA nanotracers (right column), using the peak arrival times of the BTCs shown in Figure 2. Tracers are injected at L3 and L5 in injection well MC1 and sampled at Ch4 and Ch5 in sampling well MC3. No tracer was detected in channels Ch1−Ch3, as discussed in the main text. (a and b) Vertical cross sections, showing the 2D hydraulic conductivity field, *K*. (c and d) Corresponding null-space energy maps of a and b, respectively, where the white areas in a and b represent the unreliable values of the tomogram (hydraulic conductivities), where the null-space energy is larger than the cutoff value of 0.99. The groundwater table is indicated by a blue-dashed line.

BTCs in Ch5 also exhibit an earlier first arrival for the GM2-DNA nanotracer than for sulforhodamine B, however, the peak arrival times are similar. Comparing the BTCs of the GM2-DNA nanotracer with sulforhodamine B in Figure 2, we observe a similar increase in tracer concentrations, however, the trends of the falling limbs are different. The GM2-DNA nanotracer shows a stronger concentration decrease and shorter tail. We further evaluate the tracers' transport and attenuation characteristics employing temporal moment analyses of their BTCs (columns 5−7 in Table 1), where the zeroth moment measures mass recovery, the first moment assesses the mean residence time of the tracer mass centroid, and the second moment indicates the spreading of the tracer. Compared to sulforhodamine B, the GM2-DNA nanotracer exhibits higher mass recovery (mass recovery ratio $\gtrsim 1$), travels at a greater velocity (mean residence time ratio < 1), and is less dispersive (dispersion ratio $\lesssim 1$). Note that in this study, the mass of the GM2-DNA nanotracer is 20 times smaller than that of sulforhodamine B. The relatively low mass recovery of sulforhodamine B is likely caused by adsorption.[70,71] In Ch5, the dispersion ratio of the GM2-DNA nanotracer and sulforhodamine B is with 1.04 slightly larger than 1, which results from two factors: One, the second moment calculation more heavily weighs later times, and two, the tail of the GM2-DNA nanotracer BTC rebounds to slightly higher concentrations. This slight rebound is likely due to density effects (DNA nanotracers have a density about twice that of groundwater), which induce the settling of nanotracers toward Ch5 at the later time. The observed higher travel velocity and lower dispersivity of DNA nanotracers are consistent with previous studies.[50,52−54] Due to the particle size exclusion effect,[72] the particulate DNA nanotracers can only travel through pores of a minimum size, theoretically given by the particle size. Such larger pores tend to promote fluid flow velocities that are larger than the mean fluid flow velocity. As a result, DNA nanotracers travel at velocities that are generally higher than the mean fluid flow velocity, which can be an advantage when conducting tracer tomography, as explained next.

Tracer Tomography. To assess the potential of DNA nanotracers to be used to construct tomographic inversions, two separate tomographic inversions are conducted, one with the solute dye tracers and one with the particulate DNA nanotracers. Three BTCs are used to invert the dye tracer data, which is sufficient for tomographic reconstructions. The three BTCs include two BTCs of sulforhodamine B, traveling from L3 to Ch4 and from L3 to Ch5, and one BTC of Na-naphthionate, traveling from L5 to Ch5. However, only two BTCs (GM2-DNA nanotracer, traveling from L3 to Ch4 and from L3 to Ch5) are obtained from the DNA nanotracer test, i.e., both from the same injection point, L3. A limited number of BTCs and single-source BTCs can strongly reduce the

DOI: 10.1021/acs.est.8b04367
Environ. Sci. Technol. XXXX, XXX, XXX−XXX

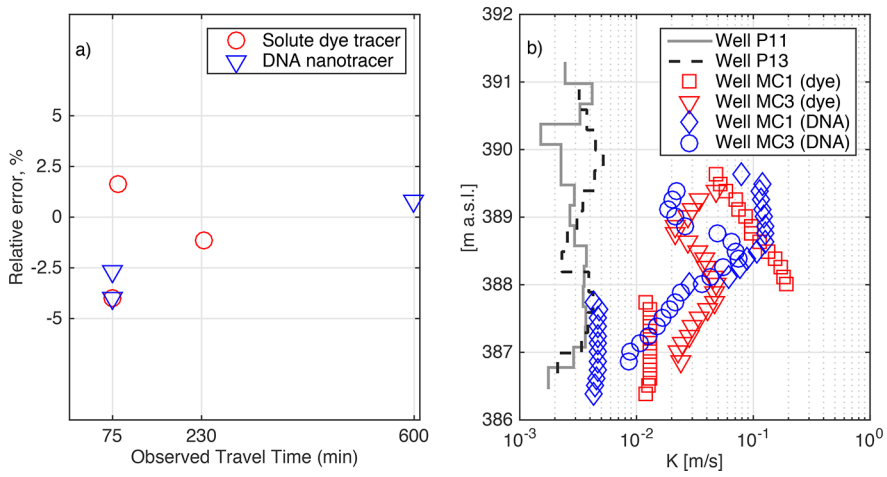

Figure 4. (a) Relative differences in percentage between the observed and the computed travel times, after convergence of the tomographic inversion. (b) Comparison of hydraulic conductivity profiles in different wells. Profiles in wells P11 and P13 were reported by Jiménez et al.[31] Profiles in wells MC1 and MC3 (dye) are extracted from the *K*-tomogram shown in Figure 3a. Profiles in wells MC1 and MC3 (DNA) are extracted from the *K*-tomogram shown in Figure 3b.

quality of an inversion and the extent of the reconstructed profile. For this reason, the DNA tracer travel time data are extended to include one additional travel time (i.e., a virtual travel time) to represent the limited, but nonzero, connectivity between the bottom source, L5, and the bottom receiver, Ch5. This virtual travel time can be arbitrary but in general is estimated using a theoretical maximum value. Based on previous estimates of a minimum $K = 6 \times 10^{-4}$ m/s at the Widen site,[32] a maximum virtual travel time of 600 min is calculated here for a straight transport pathway between L5 and Ch5 (eq 1). Employing this approximation, it is impossible to determine the actual value of the low-*K* zone; however, the approximation enables assessing the zone's geometry. Three breakthrough times (i.e., peak arrival times) are used in the dye tracer inversion, namely 85 min for sulforhodamine B between L3 and Ch4, 75 min for sulforhodamine B between L3 and Ch5, and 233 min for Na-naphthionate between L5 and Ch5 (Figure 2). Similarly three breakthrough times are used in the DNA nanotracer inversion, namely 75 min for GM2-DNA between L3 and Ch4, 74 min for GM2-DNA between L3 and Ch5, and 600 min for the virtual tracer between L5 and Ch5 (Figure 2). An initial grid size of 0.5 m × 0.5 m is used for the inversion calculation. Later the grid is staggered 3 times so that a higher grid resolution of 0.125 m × 0.125 m is reached (Figure 3). During the inversion, the porosity is fixed at 0.25, which has been reported for the Widen site.[32] The absolute relative differences between the computed and the observed travel times are ≤4%, once the inversion calculation has converged (Figure 4a).

The tomographic inversion is sensitive to regions that exhibit large hydraulic conductivities, *K*, where the majority of the tracer transport occurs and where, in the case of the particulate DNA nanotracers, size exclusion effects are negligible. This makes nanoparticle-based tracer transport particularly suitable for early travel time based tracer tomography, as regions that are not reached by the tracers do not affect tracer travel times. To eliminate unrealistic *K* values, proposed by the inversion procedure for these areas, the null-space energy map is calculated to characterize the reliability of the tomographic reconstruction. The null-space energy map is determined from the reconstructed transport trajectories by a singular value decomposition of the tomography matrix.[45] The resulting null-space energy values are between 0 and 1, where higher values indicate larger uncertainties. When the tomographic reconstruction only uses a few source-receiver combinations, the calculated null-space energy values are generally high. This is often the case in field applications, where the amount of available information is limited.[32] Here, the null-space energy map is used to mask the unreliable parts of the tomogram. Because of the limited number of source-receiver combinations, we use a cutoff value of 0.99 (Figure 3c and d).

Panels a and b in Figure 3 show the resultant 2D hydraulic conductivity, *K*, field between the injection well (MC1) and the observation well (MC3). Our inverted hydraulic conductivities are in the range of $0.004 \leq K \leq 0.1$ m/s, i.e., approximately 1 order of magnitude larger than those typically obtained from slug tests at the same location (Figure 4b).[31,73] Both of our tomographic reconstructions yield an upper zone with a larger hydraulic conductivity of $0.03 \leq K \leq 0.1$ m/s and a deeper zone with a smaller hydraulic conductivity of $0.004 \leq K \leq 0.01$ m/s. This observation agrees with the work of Coscia et al.,[21] who showed that the highest *K* values at the site occur at a depth of about 388 m and are caused by a thick gravel-rich layer. This finding is also supported by the work of Somogyvári and Bayer,[32] who conducted thermal tracer tomography at the Widen site, adjacent to these profiles, between wells P11 and MC1 (Figure 1), yielding a comparably large *K* feature in the aquifer. The slightly earlier arrival times of the DNA nanotracers, compared to the solute dye tracers, employed in our study, do not result in significantly larger *K* values. In contrast, the lack of tracer arrival near the bottom of the sampling well (MC3), where a DNA nanotracer travel time is only estimated, results in much lower *K*-values for the DNA nanotracer tomogram, compared to the solute dye tracer tomogram (Figure 3). Nonetheless, the colloidal DNA nanotracers and the solute dye tracers yield very similar tomographic inversion results, which is not surprising, given that the tracer travel times, obtained from their BTCs, are similar as well (Figure 2).

The presented field experiment shows encouraging potential for multisource−multireceiver tomographic inversions, em-

DOI: 10.1021/acs.est.8b04367
Environ. Sci. Technol. XXXX, XXX, XXX−XXX

ploying particulate DNA-labeled nanotracers, as these tracers exhibit low detection limits, relatively high mass recovery rates, little dispersion, and no susceptibility to background noise (due to the possibility to generate new, unique DNA labels for each DNA nanotracer field test). To the best of our knowledge, our study represents the first field demonstration of such a DNA-labeled, nanotracer-based tomographic inversion and interpretation. The development of this approach is still in the beginning stages. Several issues related to the applicability of the presented methodology have yet to be addressed, including (1) incorporating the influence of particle velocity variations on particle retention[74] in tomographic inversions; (2) considering tomographic inversions that integrate the temporal moments of BTCs;[18] (3) developing neutrally buoyant[22] nanotracers (such as hollow nanotracers); and (4) further improving the chemical robustness for studies in much larger reservoirs that exhibit elevated temperatures.[46,63] Nevertheless, the presented results suggest that determinations of hydraulic parameter fields, such as hydraulic conductivity fields, is possible, also at high resolutions (not investigated here), employing particulate DNA nanotracer tomography, as a virtually infinite number of differently DNA-labeled nanotracers can be used simultaneously. This capability has positive implications, for example, for hydrogeologic, petroleum engineering, and geothermal energy investigations, particularly with respect to resolving preferential flow paths or the heterogeneity of contact surfaces or by enabling source zone characterizations of dense nonaqueous phase liquids.

■ ASSOCIATED CONTENT

Supporting Information

The Supporting Information is available free of charge on the ACS Publications website at DOI: 10.1021/acs.est.8b04367.

Further information about DNA nanotracer characterization and BTCs in other sampling channels in well MC3 (PDF)

■ AUTHOR INFORMATION

Corresponding Author

*E-mail: xkong@ethz.ch.

ORCID

Xiang-Zhao Kong: 0000-0001-6254-2428

Wendelin J. Stark: 0000-0002-8957-7687

Notes

The authors declare the following competing financial interest(s): G.M. and W.J.S. declare financial interest in the form of technology commercialization through Haelixa AG, of which they are shareholders.

■ ACKNOWLEDGMENTS

The Werner Siemens Foundation (Werner Siemens-Stiftung) is thanked by M.O.S. for its support of the Geothermal Energy and Geofluids Group at ETH Zurich. We also thank N. Knornschild for his invaluable technical contributions in the GEG group laboratory and in the field. Finally, we thank the three anonymous reviewers and the editor for their excellent comments and helpful suggestions that greatly improved this paper.

■ REFERENCES

(1) Theis, C. V. The relation between the lowering of the Piezometric surface and the rate and duration of discharge of a well using groundwater storage. *Trans., Am. Geophys. Union* **1935**, *16*, 519−524.

(2) Cooper, H. H.; Jacob, C. E. A generalized graphical method for evaluating formation constants and summarizing well field history. *Trans., Am. Geophys. Union* **1946**, *27*, 526−534.

(3) Jim Yeh, T. C.; Lee, C. H. Time to change the way we collect and analyze data for aquifer characterization. *Groundwater* **2007**, *45*, 116−118.

(4) Alexander, S. C.; Saar, M. O. Improved Characterization of Small "u" for Jacob Pumping Test Analysis Methods. *Groundwater* **2012**, *50*, 256−265.

(5) Davis, S. N.; Thompson, G. M.; Bentley, H. W.; Stiles, G. GroundWater Tracers A Short Review. *Groundwater* **1980**, *18*, 14−23.

(6) Kaess, W. *Tracing technique in geohydrology in Rep. of Invest. 9617*; Balkema: Rotterdam, 1998; p 581.

(7) Leibundgut, C.; Maloszewski, P.; Külls, C. *Tracers in Hydrology*; Wiley, 2009; pp 1−415.

(8) Anderson, M. P. Heat as a ground water tracer. *Ground Water* **2005**, *43*, 951−68.

(9) Saar, M. O.; Castro, M. C.; Hall, C. M.; Manga, M.; Rose, T. P. Quantifying magmatic, crustal, and atmospheric helium contributions to volcanic aquifers using all stable noble gases: Implications for magmatism and groundwater flow. *Geochem., Geophys., Geosyst.* **2005**, *6*, Q03008.

(10) Saar, M. O. Review: Geothermal heat as a tracer of large-scale groundwater flow and as a means to determine permeability fields. *Hydrogeol. J.* **2011**, *19*, 31−52.

(11) Gottardi, R.; Kao, P. H.; Saar, M. O.; Teyssier, C. Effects of permeability fields on fluid, heat, and oxygen isotope transport in extensional detachment systems. *Geochem., Geophys., Geosyst.* **2013**, *14*, 1493−1522.

(12) Luhmann, A. J.; Covington, M. D.; Myre, J. M.; Perne, M.; Jones, S. W.; Alexander, E. C.; Saar, M. O. Thermal damping and retardation in karst conduits. *Hydrol. Earth Syst. Sci.* **2015**, *19*, 137−157.

(13) Dasgupta, S.; Saar, M. O.; Edwards, R. L.; Shen, C. C.; Cheng, H.; Alexander, E. C. Three thousand years of extreme rainfall events recorded in stalagmites from Spring Valley Caverns, Minnesota. *Earth Planet. Sci. Lett.* **2010**, *300*, 46−54.

(14) Covington, M. D.; Luhmann, A. J.; Wicks, C. M.; Saar, M. O. Process length scales and longitudinal damping in karst conduits. *Journal of Geophysical Research: Earth Surface* **2012**, *117*, 1−19.

(15) Saar, M. O.; Manga, M. Depth dependence of permeability in the Oregon Cascades inferred from hydrogeologic, thermal, seismic, and magmatic modeling constraints. *Journal of Geophysical Research B: Solid Earth* **2004**, *109*, 1−19.

(16) Walsh, S. D. C.; Saar, M. O. Macroscale lattice-Boltzmann methods for low Peclet number solute and heat transport in heterogeneous porous media. *Water Resour. Res.* **2010**, *46*, 1−15.

(17) Yeh, T.-C. J.; Zhu, J. Hydraulic/partitioning tracer tomography for characterization of dense nonaqueous phase liquid source zones. *Water Resour. Res.* **2007**, *43*, W06435.

(18) Zhu, J.; Cai, X.; Jim Yeh, T.-C. Analysis of tracer tomography using temporal moments of tracer breakthrough curves. *Adv. Water Resour.* **2009**, *32*, 391−400.

(19) Lange, J.; Schuetz, T.; Gregoire, C.; Elsässer, D.; Schulz, R.; Passeport, E.; Tournebize, J. Multi-tracer experiments to characterise contaminant mitigation capacities for different types of artificial wetlands. *Int. J. Environ. Anal. Chem.* **2011**, *91*, 768−785.

(20) Doetsch, J.; Linde, N.; Coscia, I.; Greenhalgh, S. A.; Green, A. G. Zonation for 3D aquifer characterization based on joint inversions of multimethod crosshole geophysical data. *Geophysics* **2010**, *75*, G53−G64.

(21) Coscia, I.; Greenhalgh, S. A.; Linde, N.; Doetsch, J.; Marescot, L.; Günther, T.; Vogt, T.; Green, A. G. 3D crosshole ERT for aquifer

DOI: 10.1021/acs.est.8b04367
Environ. Sci. Technol. XXXX, XXX, XXX−XXX

characterization and monitoring of infiltrating river water. *Geophysics* **2011**, *76*, G49−G59.
(22) Shakas, A.; Linde, N.; Baron, L.; Selker, J.; Gerard, M.-F.; Lavenant, N.; Bour, O.; Le Borgne, T. Neutrally buoyant tracers in hydrogeophysics: Field demonstration in fractured rock. *Geophys. Res. Lett.* **2017**, *44*, 3663−3671.
(23) Butler, J.; McElwee, C. D.; Bohling, G. C. Pumping tests in networks of multilevel sampling wells: Motivation and methodology. *Water Resour. Res.* **1999**, *35*, 3553−3560.
(24) Illman, W. A.; Liu, X.; Takeuchi, S.; Yeh, T.-C. J.; Ando, K.; Saegusa, H. Hydraulic tomography in fractured granite: Mizunami Underground Research site, Japan. *Water Resour. Res.* **2009**, *45*, W01406.
(25) Berg, S. J.; Illman, W. A. Three-dimensional transient hydraulic tomography in a highly heterogeneous glaciofluvial aquifer-aquitard system. *Water Resour. Res.* **2011**, *47*, W10507.
(26) Brauchler, R.; Hu, R.; Hu, L.; Jiménez, S.; Bayer, P.; Dietrich, P.; Ptak, T. Rapid field application of hydraulic tomography for resolving aquifer heterogeneity in unconsolidated sediments. *Water Resour. Res.* **2013**, *49*, 2013−2024.
(27) Cardiff, M.; Barrash, W.; Kitanidis, P. K. Hydraulic conductivity imaging from 3-D transient hydraulic tomography at several pumping/observation densities. *Water Resour. Res.* **2013**, *49*, 7311−7326.
(28) Hu, L.; Bayer, P.; Alt-Epping, P.; Tatomir, A.; Sauter, M.; Brauchler, R. Time-lapse pressure tomography for characterizing CO_2 plume evolution in a deep saline aquifer. *Int. J. Greenhouse Gas Control* **2015**, *39*, 91−106.
(29) Zhao, Z.; Illman, W. A. Three-dimensional imaging of aquifer and aquitard heterogeneity via transient hydraulic tomography at a highly heterogeneous field site. *J. Hydrol.* **2018**, *559*, 392−410.
(30) Brauchler, R.; Böhm, G.; Leven, C.; Dietrich, P.; Sauter, M. A laboratory study of tracer tomography. *Hydrogeol. J.* **2013**, *21*, 1265−1274.
(31) Jiménez, S.; Mariethoz, G.; Brauchler, R.; Bayer, P. Smart pilot points using reversible-jump Markov-chain Monte Carlo. *Water Resour. Res.* **2016**, *52*, 3966−3983.
(32) Somogyvári, M.; Bayer, P. Field validation of thermal tracer tomography for reconstruction of aquifer heterogeneity. *Water Resour. Res.* **2017**, *53*, 5070−5084.
(33) Ghergut, I.; McDermott, C.; Herfort, M.; Sauter, M.; Kolditz, O. Reducing ambiguity in fractured-porous media characterization using single-well tracer tests. *ModelCARE-2005: From Uncertainty to Decision Making*; 2006; pp 17−24.
(34) Wagner, V.; Li, T.; Bayer, P.; Leven, C.; Dietrich, P.; Blum, P. Thermal tracer testing in a sedimentary aquifer: field experiment (Lauswiesen, Germany) and numerical simulation. *Hydrogeol. J.* **2014**, *22*, 175−187.
(35) Illman, W. A.; Berg, S. J.; Liu, X.; Massi, A. Hydraulic/partitioning tracer tomography for DNAPL source zone characterization: Small-scale sandbox experiments. *Environ. Sci. Technol.* **2010**, *44*, 8609−8614.
(36) Mueller, M. H.; Alaoui, A.; Kuells, C.; Leistert, H.; Meusburger, K.; Stumpp, C.; Weiler, M.; Alewell, C. Tracking water pathways in steep hillslopes by δ18O depth profiles of soil water. *J. Hydrol.* **2014**, *519*, 340−352.
(37) Bero, N. J.; Ruark, M. D.; Lowery, B. Bromide and chloride tracer application to determine sufficiency of plot size and well depth placement to capture preferential flow and solute leaching. *Geoderma* **2016**, *262*, 94−100.
(38) Liao, R.; Yang, P.; Wu, W.; Luo, D.; Yang, D. A DNA tracer system for hydrological environment investigations. *Environ. Sci. Technol.* **2018**, *52*, 1695−1703.
(39) Olsen, J.; Seierstad, I.; Vinther, B.; Johnsen, S.; Heinemeier, J. Memory effect in deuterium analysis by continuous flow isotope ratio measurement. *Int. J. Mass Spectrom.* **2006**, *254*, 44−52.
(40) Kirchner, J. W.; Feng, X.; Neal, C. Catchment-scale advection and dispersion as a mechanism for fractal scaling in stream tracer concentrations. *J. Hydrol.* **2001**, *254*, 82−101.
(41) Kung, K.-J.; Kladivko, E.; Gish, T.; Steenhuis, T.; Bubenzer, G.; Helling, C. Quantifying preferential flow by breakthrough of sequentially applied tracers silt loam soil. *Soil Sci. Soc. Am. J.* **2000**, *64*, 1296−1304.
(42) Rona, M.; Gasser, G.; Negev, I.; Pankratov, I.; Elhanany, S.; Lev, O.; Gvirtzman, H. A 3-D hydrologic transport model of a water recharge system using carbamazepine and chloride as tracers. *Water Resour. Res.* **2014**, *50*, 4220−4241.
(43) Field, M. S. Assessing aquatic ecotoxicological risks associated with fluorescent dyes used for water-tracing studies. *Environmental & Engineering Geoscience* **2005**, *11*, 295−308.
(44) Aiken, G. R.; Hsu-Kim, H.; Ryan, J. N. Influence of Dissolved Organic Matter on the Environmental Fate of Metals, Nanoparticles, and Colloids. *Environ. Sci. Technol.* **2011**, *45*, 3196−3201 PMID: 21405118 .
(45) Jiménez, S.; Brauchler, R.; Bayer, P. A new sequential procedure for hydraulic tomographic inversion. *Adv. Water Resour.* **2013**, *62*, 59−70.
(46) Paunescu, D.; Puddu, M.; Soellner, J. O. B.; Stoessel, P. R.; Grass, R. N. Reversible DNA encapsulation in silica to produce ROS-resistant and heat-resistant synthetic DNA 'fossils'. *Nat. Protoc.* **2013**, *8*, 2440−2448.
(47) Puddu, M.; Paunescu, D.; Stark, W. J.; Grass, R. N. Magnetically recoverable, thermostable, hydrophobic DNA/silica encapsulates and their application as invisible oil tags. *ACS Nano* **2014**, *8*, 2677−2685.
(48) Mahler, B. J.; Winkler, M.; Bennett, P.; Hillis, D. M. DNA-labeled clay: a sensitive new method for tracing particle transport. *Geology* **1998**, *26*, 831−834.
(49) Sharma, A. N.; Luo, D.; Walter, M. T. Hydrological tracers using nanobiotechnology: proof of concept. *Environ. Sci. Technol.* **2012**, *46*, 8928−8936.
(50) Aquilanti, L.; Clementi, F.; Landolfo, S.; Nanni, T.; Palpacelli, S.; Tazioli, A. A DNA tracer used in column tests for hydrogeology applications. *Environ. Earth Sci.* **2013**, *70*, 3143−3154.
(51) Mora, C. A.; Paunescu, D.; Grass, R. N.; Stark, W. J. Silica particles with encapsulated DNA as trophic tracers. *Mol. Ecol. Resour.* **2015**, *15*, 231−241.
(52) Pang, L.; Robson, B.; Farkas, K.; McGill, E.; Varsani, A.; Gillot, L.; Li, J.; Abraham, P. Tracking effluent discharges in undisturbed stony soil and alluvial gravel aquifer using synthetic DNA tracers. *Sci. Total Environ.* **2017**, *592*, 144−152.
(53) Sabir, I. H.; Torgersen, J.; Haldorsen, S.; Aleström, P. DNA tracers with information capacity and high detection sensitivity tested in groundwater studies. *Hydrogeol. J.* **1999**, *7*, 264−272.
(54) Ptak, T.; Piepenbrink, M.; Martac, E. Tracer tests for the investigation of heterogeneous porous media and stochastic modelling of flow and transporta review of some recent developments. *J. Hydrol.* **2004**, *294*, 122−163.
(55) Foppen, J. W.; Orup, C.; Adell, R.; Poulalion, V.; Uhlenbrook, S. Using multiple artificial DNA tracers in hydrology. *Hydrological Processes* **2011**, *25*, 3101−3106.
(56) Foppen, J. W.; Seopa, J.; Bakobie, N.; Bogaard, T. Development of a methodology for the application of synthetic DNA in stream tracer injection experiments. *Water Resour. Res.* **2013**, *49*, 5369−5380.
(57) Dahlke, H. E.; Williamson, A. G.; Georgakakos, C.; Leung, S.; Sharma, A. N.; Lyon, S. W.; Walter, M. T. Using concurrent DNA tracer injections to infer glacial flow pathways. *Hydrological Processes* **2015**, *29*, 5257−5274.
(58) Bovolin, V.; Cuomo, A.; Guida, D.; Foppen, J. Using artificial DNA as tracer in a bedrock river of the Middle Bussento Karst System (Cilento, Vallo Diano and Alburni European & Global Geopark, southern Italy). *Proceedings of the 7th International Conference on Engineering Mechanics, Structures, Engineering Geology (EMESEG14)*, Salerno, Italy, 2014; pp 3−5.
(59) Sabir, I. H.; Haldorsen, S.; Torgersen, J.; Alestrom, P.; Gaut, S.; Colleuille, H.; Pedersen, T. S.; Kitterod, N.-O.; Alestrom, P. *Synthetic DNA tracers: examples of their application in water related studies*;

DOI: 10.1021/acs.est.8b04367
Environ. Sci. Technol. XXXX, XXX, XXX−XXX

International Association of Hydrological Sciences, 2000; pp 159−165.
(60) Sabir, I. H.; Alestrom, P.; Haldorsen, S. Use of Synthetic DNA as New Tracers for Tracing Groungwater Flow and Multiple Contaminants. *J. Appl. Sci.* **2001**, *1*, 233−238.
(61) Grass, R. N.; Schalchli, J.; Paunescu, D.; Soellner, J. O.; Kaegi, R.; Stark, W. J. Tracking trace amounts of submicrometer silica particles in wastewaters and activated sludge using silica-encapsulated DNA barcodes. *Environ. Sci. Technol. Lett.* **2014**, *1*, 484−489.
(62) Mikutis, G.; Mora, C. A.; Puddu, M.; Paunescu, D.; Grass, R. N.; Stark, W. J. DNA-Based Sensor Particles Enable Measuring Light Intensity in Single Cells. *Adv. Mater.* **2016**, *28*, 2765−2770.
(63) Mikutis, G.; Deuber, C. A.; Schmid, L.; Kittilä, A.; Lobsiger, N.; Puddu, M.; Asgeirsson, D. O.; Grass, R. N.; Saar, M. O.; Stark, W. J. Silica encapsulated DNA-based tracers for aquifer characterization. *Environ. Sci. Technol.* **2018**, *52*, 12142.
(64) Wang, S.; Edwards, I. M.; Clarens, A. F. Wettability phenomena at the CO2−brine−mineral interface: implications for geologic carbon sequestration. *Environ. Sci. Technol.* **2013**, *47*, 234−241.
(65) Bustamante, C.; Smith, S. B.; Liphardt, J.; Smith, D. Single-molecule studies of DNA mechanics. *Curr. Opin. Struct. Biol.* **2000**, *10*, 279−285.
(66) Valocchi, A. J. Validity of the local equilibrium assumption for modeling sorbing solute transport through homogeneous soils. *Water Resour. Res.* **1985**, *21*, 808−820.
(67) Somogyvari, M.; Bayer, P.; Brauchler, R. Travel-time-based thermal tracer tomography. *Hydrol. Earth Syst. Sci.* **2016**, *20*, 1885−1901.
(68) Vasco, D.; Datta-Gupta, A. Asymptotic solutions for solute transport: A formalism for tracer tomography. *Water Resour. Res.* **1999**, *35*, 1−16.
(69) Jackson, M. J.; Tweeton, D. R. *3DTOM, Three-dimensional Geophysical Tomography in Rep. of Invest. 9617*; 1996; p 84.
(70) Smart, P.; Laidlaw, I. An evaluation of some fluorescent dyes for water tracing. *Water Resour. Res.* **1977**, *13*, 15−33.
(71) Magal, E.; Weisbrod, N.; Yakirevich, A.; Yechieli, Y. The use of fluorescent dyes as tracers in highly saline groundwater. *J. Hydrol.* **2008**, *358*, 124−133.
(72) Sirivithayapakorn, S.; Keller, A. Transport of colloids in saturated porous media: A pore-scale observation of the size exclusion effect and colloid acceleration. *Water Resour. Res.* **2003**, *39*, 1109−1119.
(73) Diem, S.; Vogt, T.; Hoehn, E. Räumliche charakterisierung der hydraulischen leitfähigkeit in alluvialen schotter-grundwasserleitern: Ein methodenvergleich. *Grundwasser* **2010**, *15*, 241−251.
(74) Sasidharan, S.; Bradford, S. A.; Torkzaban, S.; Ye, X.; Vanderzalm, J.; Du, X.; Page, D. Unraveling the complexities of the velocity dependency of E. coli retention and release parameters in saturated porous media. *Sci. Total Environ.* **2017**, *603*, 406−415.

DOI: 10.1021/acs.est.8b04367
Environ. Sci. Technol. XXXX, XXX, XXX−XXX